JOURNAL OF GEOPHYSICAL RESEARCH, VOL. 105, NO. B7, PAGES 16,371–16,389, JULY 10, 2000

Failure mode and weakening effect of water on sandstone

Patrick Baud

Department of Geosciences, State University of New York at Stony Brook

Wenlu Zhu

Department of Geology and Geophysics, Woods Hole Oceanographic Institute, Woods Hole, Massachusetts

Teng-fong Wong

Department of Geosciences, State University of New York at Stony Brook

Abstract. Previous studies have shown that brittle strength of a rock is generally reduced in the presence of water. However, for siliciclastic rocks, there is a paucity of data on the water-weakening behavior in the cataclastic flow regime. To compare the weakening effect of water in the brittle faulting and cataclastic flow regime, triaxial compression experiments were conducted on the Berea, Boise, Darley Dale, and Gosford sandstones (with nominal porosities ranging from 11% to 35%) under nominally dry and saturated conditions at room temperature. Inelastic behavior and failure mode of the nominal dry samples were qualitatively similar to those of water-saturated samples. At elevated pressures, shear localization was inhibited, and all the samples failed by strain hardening. The compactive yield strengths (associated with the onset of shear-enhanced compaction) in the saturated samples were lower than those in the dry samples deformed under comparable pressure conditions by 20% to 70%. The reductions of brittle strength in the presence of water ranged from 5% to 17%. The water-weakening effects were most and least significant in the Gosford and Berea sandstones, respectively. The relation between water weakening and failure mode is consistently explained by micromechanical models formulated on the basis that the specific surface energy in the presence of water is lowered than that in vacuum by the ratio λ. In accordance with the Hertzian fracture model the initial yield stress in the compactive cataclastic flow regime scales with the grain-crushing pressure, which is proportional to $\lambda^{3/2}$. In the brittle faulting regime, damage mechanics models predict that the uniaxial compressive strength scales with $\lambda^{1/2}$. In the presence of water the confined brittle strength is lower due to reductions of both the specific surface energy and friction coefficient.

1. Introduction

Aqueous pore fluid exerts significant mechanical and chemical effects on virtually all crustal processes. Previous studies have shown that brittle strength of a rock is generally reduced in the presence of water. The water-weakening effect may arise from two mechanisms. The mechanical role of pressurized pore fluid tends to weaken and embrittle rocks [*Paterson*, 1978], and the chemical influence of pore fluids is to further weaken the rock through a reduction of surface free energy [*Rehbinder et al.*, 1948; *Orowan*, 1944], a subcritical cracking mechanism such as stress corrosion [*Atkinson and Meredith*, 1987], or both combined.

Previous experimental studies have focused on the brittle strength, and the data suggest that the water-weakening effect is quite variable. *Lajtai et al.* [1987] and *Hadizadeh and Law* [1991] observed appreciable reductions of the unconfined strength in Lac du Bonnet granite and Pennant sandstone in the presence of water. Triaxial compression experiments also show significant water weakening in the Punchbowl sandstone [*Chester and Logan*, 1986] and Tennessee sandstone [*Rutter and Mainprice*, 1978]. *Colback and Wiid* [1965] observed an almost constant water-weakening effect of ~30% in a quartzitic sandstone under triaxial compression. In contrast, *Boozer et al.* [1963] concluded that the weakening effect of water on Navajo sandstone decreased at higher pressures so that at effective pressures of 83 and 138 MPa the effect was negligible.

Unlike the brittle faulting regime, there is a paucity of data on the water-weakening behavior in the cataclastic flow regime. Stress-strain data on Berea sandstone reported by *Handin et al.* [1963] and *Bernabé and Brace* [1990] suggest a very slight weakening effect in the water-saturated samples. In contrast, *Read et al.* [1995] recently presented data from one experiment on Darley Dale sandstone that showed very significant weakening. *Zhu and Wong* [1997] observed comparable effects in Darley Dale and Berea sandstone at effective pressures ranging from 100 to 360 MPa. They also reported significant enhancement of hydrostatic and nonhydrostatic compaction in the presence of water.

It is generally recognized that although the macroscopic failure modes in the brittle faulting and cataclastic flow regimes are fundamentally different, grain-scale

Paper number 2000JB900087.
0148-0227/00/2000JB900087$09.00

microcracking is involved in both regimes. Significant advances have been made in the theoretical modeling of such microcracking processes by linear elastic fracture mechanics. While the "sliding wing crack" model [*Horii and Nemat-Nasser*, 1986; *Ashby and Sammis*, 1990; *Kemeny and Cook*, 1991] has been widely used to analyze the development of dilatancy and brittle faulting, the "Hertzian fracture" model [*Zhang et al.*, 1990b] was developed to model grain crushing and pore collapse associated with compactive cataclastic flow. The presence of water may result in marked variations of parameters such as the fracture toughness, friction coefficient, and initial damage that play key roles in these micromechanical models.

In this study, we will try to quantify the water-weakening effect as a function of pressure by comparing the mechanical deformation of sandstone samples under nominally dry and saturated conditions in the brittle faulting and cataclastic flow regimes. Triaxial compression experiments were conducted on the Gosford, Darley Dale, Berea, and Boise sandstones (with nominal porosities ranging from 11 to 35%) under "drained" conditions at room temperature. The micromechanical processes responsible for the overall reductions in brittle strength and compactive yield stress are interpreted using the wing crack and Hertzian fracture models, respectively.

2. Mechanical Data and Weakening Effect of Water

2.1. Sample Preparation

Berea, Boise, Darley Dale, and Gosford sandstones (with nominal porosities of 21%, 35%, 13%, and 11%, respectively) are used is this study. The Berea, Boise, and Darley Dale sandstones were from the same blocks studied by *Wong et al.* [1997], who have provided the petrophysical descriptions. The Gosford sandstone samples were kindly furnished by S. F. Cox of the Australian National University, and the petrophysical properties are expected to be similar to the samples studied by *Edmond and Paterson* [1972].

The samples were cored perpendicular to their sedimentary bedding and then ground to a cylindrical shape, with diameter of 18.4 mm and length 38.1 mm. For a "wet" experiment the sample was saturated with distilled water and jacketed with copper foil and then positioned between two steel end-plugs, one of which has a piezoelectric transducer (PZT-7, 5.0-mm diameter, 1-MHz longitudinal resonant frequency) on its flat surface, and the other one has a concentric hole at the center for fluid access to the pore pressure system. Heat-shrink polyolefine tubings were used to separate the sample from confining pressure medium.

For a nominally dry test the sample was dried in vacuum for a week at 80°C. Special care was taken during sample preparation to avoid incorporating moisture on the surface. For the Darley Dale and Berea sandstone samples, longitudinal and transverse strains were measured by two electric resistance strain gauges (type FAE-50-12-P for strains up to 15%). To circumvent the problem of breakage of strain gauges from stress-induced pore collapse, a thin layer of fast cured epoxy was first applied to fill up the surface pores before jacketing the sample with thin copper foil (of thickness 0.05 mm). The strain gauges were then mounted in orthogonal directions on the copper jacket. Even with this approach we had extreme difficulties with mounting strain gauges on the Boise sandstone. Only axial strain data inferred from a displacement transducer (DCDT) measurements are available for this sandstone with the highest porosity.

2.2. Experimental Procedure

The jacketed samples were stressed in the conventional triaxial configuration at room temperature. Kerosene was used as the confining medium. The samples were subjected to confining pressures ranging from 10 to 550 MPa. The axial displacement was servo-controlled at a fixed rate (corresponding to a nominal strain rate of 1.3×10^{-5} s^{-1}). The confining pressure was monitored by a strain gauge pressure transducer to accuracy of 0.5 MPa. The axial load was measured with an external load cell with an accuracy of 1 kN.

To measure acoustic emission (AE) activity during the triaxial experiments, we used a piezoelectric transducer on the flat surface of a steel spacer attached to the jacketed sample. The AE signals were conditioned by a preamplifier (gain 40 dB, frequency response 1.5 kHz to 5 MHz). To distinguish AE events from electric spikes, a discriminator was used to check two characteristics of the incoming signal. The details were described by *Zhang et al.* [1990a]. For the dry samples, volumetric strain was calculated from the strain gauge data by summing the axial strain and twice the transverse strain.

Experiments on the saturated samples were conducted at a fixed pore pressure of 10 MPa under fully drained conditions. Adjustment of a pressure generator kept the pore pressure constant, and the pore volume change was recorded by monitoring the piston displacement of the pressure generator with a displacement transducer (DCDT). The porosity change was calculated from the ratio of the pore volume change to the initial bulk volume of the sample, with an uncertainty of ±0.1%. The displacement was measured outside the pressure vessel with a DCDT mounted between the moving piston and the fixed upper platen. The uncertainty of the axial displacement measurement was 10 μm.

With a knowledge of the stiffness of the loading system (2.38×10^8 N/m), the axial displacement of the saturated sample was obtained by subtracting the displacement of the loading system from the apparent displacement recorded by the DCDT, and the axial strain was calculated with reference to the initial length of the sample. To calculate the axial stress from the recorded axial force, effect of bulging was accounted for by inferring the relative increase in area of a deformed sample by subtracting the axial strain from the porosity change.

2.3. Mechanical Data

The compressive stresses and compactive strains will be taken positive. We will denote the maximum and minimum (compressive) principal stresses by σ_1 and σ_3, respectively. The pore pressure will be denoted by P_p, and the difference between the confining pressure ($P_c = \sigma_2 = \sigma_3$) and pore pressure will be referred to as the "effective pressure" P_{eff}.

2.3.1. Brittle faulting regime. Mechanical data in the brittle faulting regime for the nominally dry and saturated samples of Darley Dale and Berea sandstones are shown in Figures 1 and 2. The differential stress as a function of axial strain is shown in Figures 1a and 2a. The volumetric strain (for nominally dry samples) and porosity reduction (for

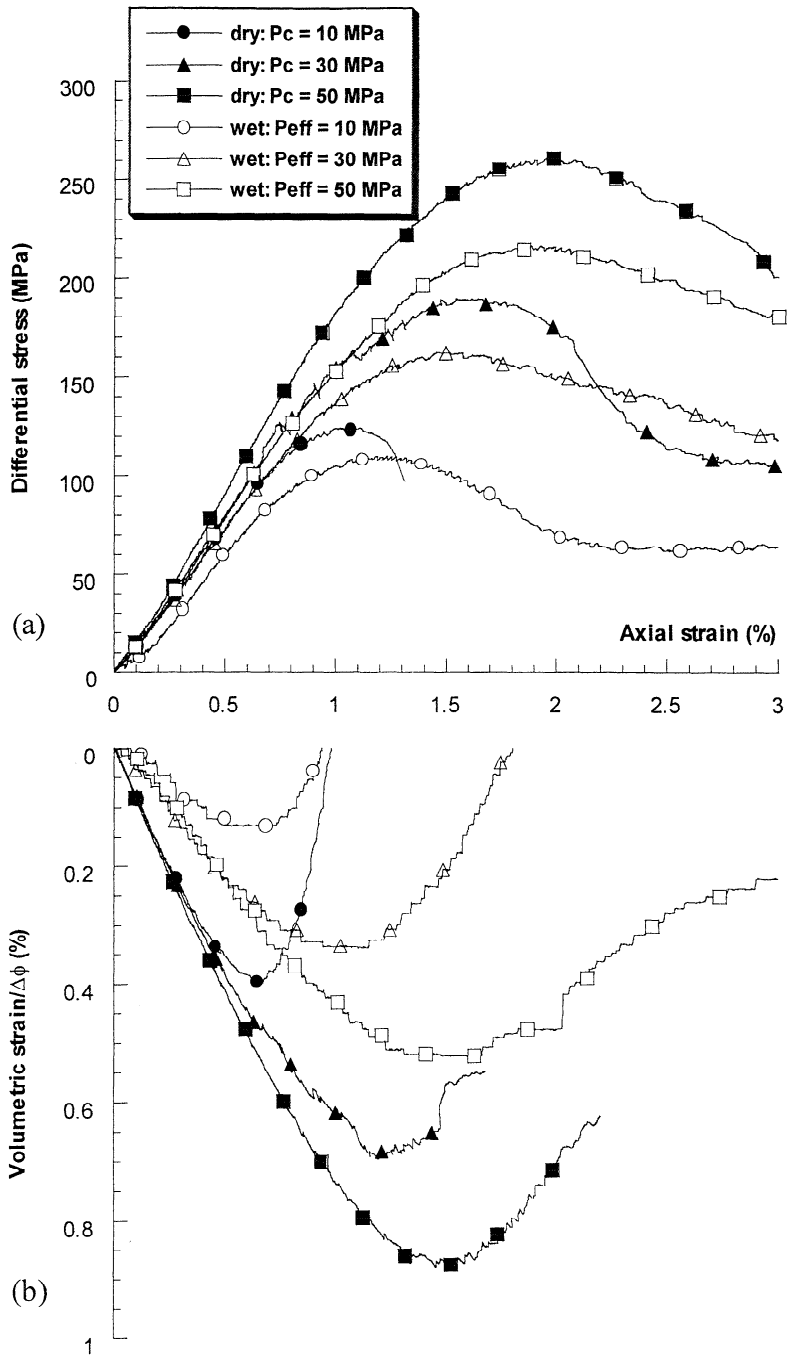

Figure 1. Mechanical data for Darley Dale sandstone samples deformed in the brittle faulting regime. (a) Differential stress and (b) volumetric strain (or porosity change) were plotted versus axial strain. The open symbols are for water-saturated samples, and the solid symbols are for the nominally dry samples.

saturated samples) are also shown as functions of axial strain in Figures 1b and 2b. Mechanical data in the brittle faulting regime for the Boise sandstone are shown in Figure 3. Since strain gauges were not employed, only data on the differential stress as a function of axial strain are available for the dry samples.

In all experiments shown in Figures 1 and 2, the differential stress attained a peak, beyond which strain softening was observed and the stress dropped to a residual level. The loading frame was sufficiently stiff that the stress drop was stable in most experiments, except for the dry Darley Dale sample deformed at a confining pressure of 10 MPa that showed a catastrophic stress drop. For all samples the porosity or volumetric strain initially decreased due to compaction, but near the peak stress it reversed to an increase indicating dilatation of the pore space. Visual inspection of postpeak samples confirmed that they failed by shear localization, with a throughgoing shear band cutting across each sample. The orientations of the shearing band were found to be at an angle of ~30° with respect to σ_1.

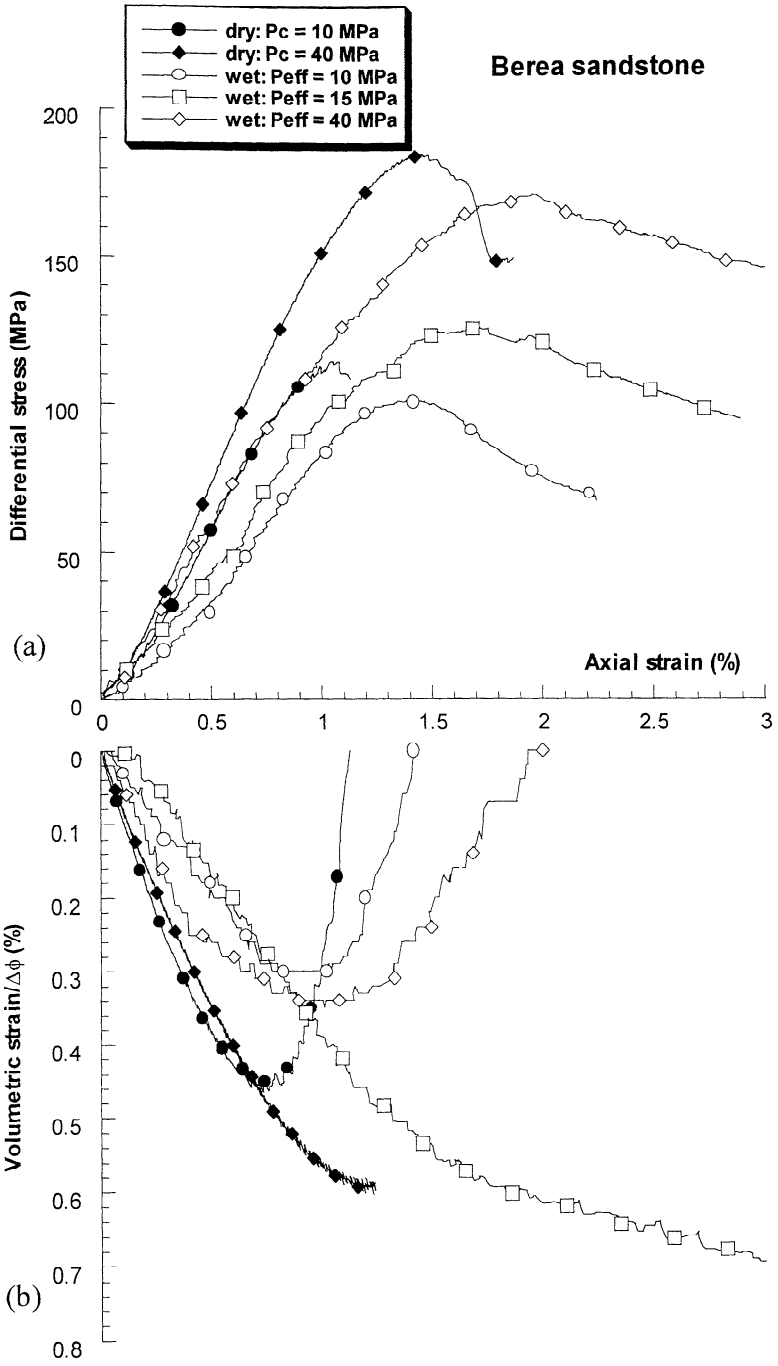

Figure 2. Mechanical data for Berea sandstone samples deformed in the brittle faulting regime. (a) Differential stress and (b) volumetric strain (or porosity change) were plotted versus axial strain. The open symbols are for water-saturated samples, and the solid symbols are for the nominally dry samples.

Overall, the mechanical data for dry and wet experiments are qualitatively the same, but generally, the postpeak behavior was more stable for a saturated sample than for a dry one at the same effective pressure. For all experiments, AE activity was not significant until after the onset of dilatancy. Subject to the limited resolution of our system, the AE activities were qualitatively similar in dry and wet experiments.

Mechanical data on Boise sandstone samples are presented in Figure 3. Since strain gauges were not employed, data on the volumetric strain are not available for the dry samples. In the presence of water our data for effective pressures between 5 and 20 MPa indicate failure mode for a transitional regime, with attainment of peak stress and shear-enhanced compaction. Dilatancy and shear localization were not evident in these saturated Boise sandstone samples. We concluded that if brittle faulting were to occur in Boise sandstone, it would be below 5 MPa of effective pressure. Owing to the limited size of the Gosford sandstone block available, we did not have any samples left for additional experiments in the brittle faulting regime.

Table 1 compiles the peak stresses attained in the experiments shown in Figures 1 to 3. In both dry and wet sandstone samples the peak stresses are positively correlated

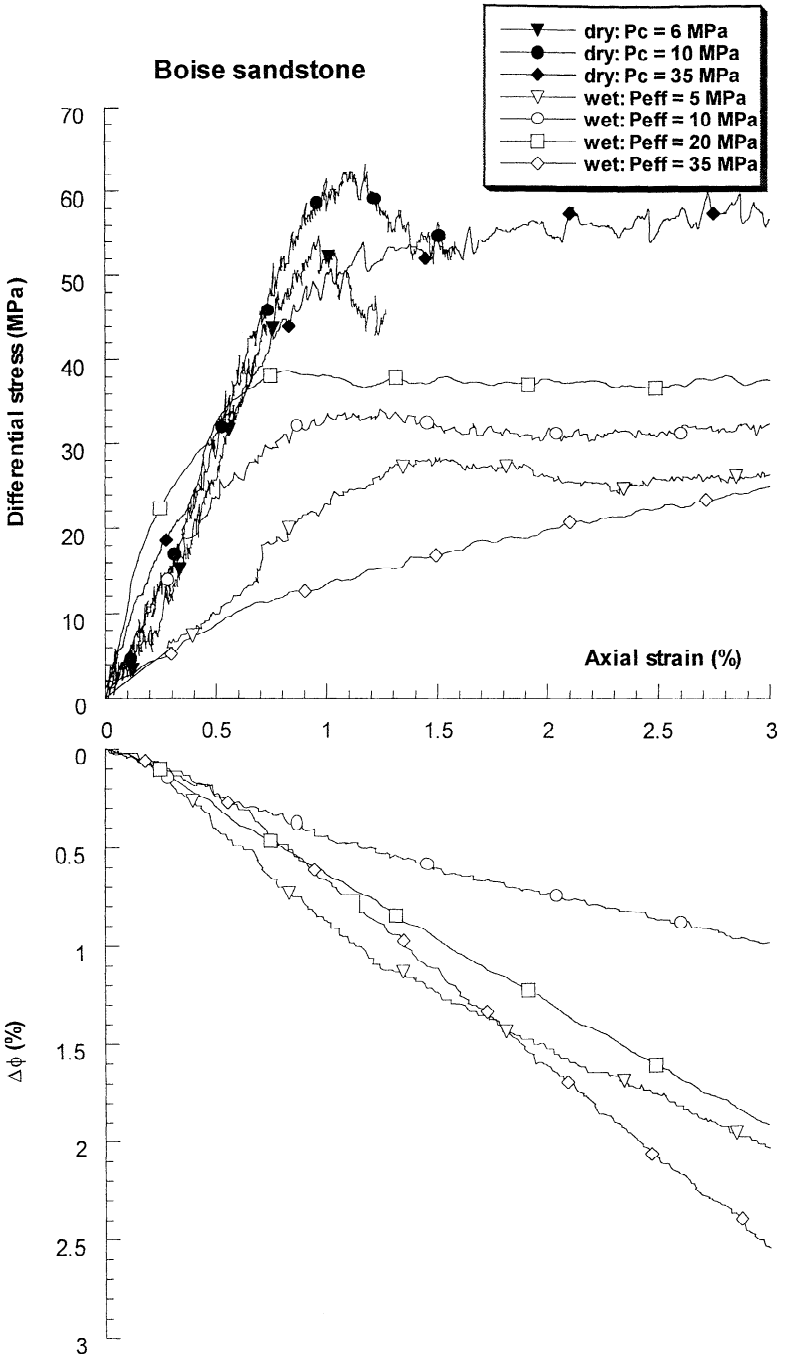

Figure 3. Mechanical data for Boise sandstone samples. Differential stress and porosity change were plotted versus axial strain. The open symbols are for water-saturated samples, and the solid symbols are for the nominally dry samples.

with effective pressures. At a given effective pressure the ratio between the peak stresses of saturated and nominally dry samples is less than unity. This ratio is compiled in Table 1. Appreciable water weakening (ranging from 5% to 17%) was observed.

2.3.2. Cataclastic flow regime. At elevated pressures, shear localization was inhibited, and all samples failed by cataclastic flow. A sample typically shows an initial linear response, followed by appreciable strain hardening and volumetric compaction, with a surge in AE activity. This regime of deformation is manifested by damage in the form of homogeneously distributed microcracking, grain crushing, and pore collapse [*Menéndez et al.*, 1996].

Mechanical data for the nominally dry and saturated samples of Boise, Darley Dale, Berea, and Gosford sandstones are presented in Figures 3 to 6. While the strain-hardening and compaction characteristics of the samples are qualitatively similar at the same effective pressure, a dry sample generally required an appreciably higher stress than a saturated sample to attain the same axial strain. Some of these

Table 1. Peak Stress, Onset of Dilatancy C' and Water Weakening for Samples That Failed by Shear Localization

Effective Pressure $\sigma_1 - P_p$, MPa	Dry: Peak Stress $\sigma_1 - \sigma_3$, MPa	Dry: Dilatancy C' $\sigma_1 - \sigma_3$, MPa	Wet: Peak Stress $\sigma_1 - \sigma_3$, MPa	Wet: Dilatancy C' $\sigma_1 - \sigma_3$, MPa	Weakening Peak(Wet) /Peak (Dry)
		Darley Dale			
10	126	54	110	37	0.88
30	190	109	163	90	0.86
50	263	174	217	143	0.83
		Berea			
10	115	32	102	36	-
15	-	-	126	39	0.89
30	-	-	159	72	-
40	186	89	177	83	0.95

quantitative differences in strain hardening and compaction behaviors were discussed in detail by *Zhu and Wong* [1997].

For saturated sandstone we used the same procedure as *Wong et al.* [1997] to identify the yield stress C^* at the onset of shear-enhanced compaction from mechanical data. Figure 7a illustrates an analogous procedure that has been adopted to pick C^* for the nominally dry samples. The triaxial compression data (for Berea sandstone at a confining pressure of 250 MPa) are plotted in the form of the mean stress $(\sigma_1 + 2\sigma_3)/3$ versus the volumetric strain. For reference, hydrostatic compression data of a dry Berea sandstone are also included. Typically, the hydrostat of a porous sandstone has an inflection point that marks the critical pressure P^* for the onset of grain crushing and pore collapse [*Zhang et al.*, 1990b].

The nonhydrostatic and hydrostatic loadings are coupled together in a triaxial compression experiment. If the volumetric strain is solely controlled by the hydrostatic stresses, then the triaxial data (solid curves) should coincide with the hydrostat (dashed curves) in Figure 7a. Deviations from the hydrostat would imply that additional volume change was induced by the deviatoric stresses. In the cataclastic flow regime the triaxial curve for a given effective pressure coincided with the hydrostat up to a critical stress state (indicated by C^* in Figure 7a), beyond which there was an accelerated decrease in volumetric strain in comparison to the hydrostat. At stress levels beyond C^* the deviatoric stress field provided significant contribution to the compactive strain, and this phenomenon is referred to as "shear-enhanced compaction" [*Curran and Carroll*, 1979; *Wong et al.*, 1997]. The initiation of compactive yield is also associated with a surge in AE activity (Figure 7a). Since no volumetric strain data are available for the dry Boise sandstone samples, we identified C^* using only this onset of AE activity.

In Table 2 we compile the values of C^* and P^* determined experimentally for the four sandstones that we used in this study; some of the data for the Berea sandstone have been taken from *Zhu and Wong* [1997]. In Figure 8 the yield stress data are also plotted in the stress space in coordinates of effective mean stress P ($= (\sigma_1 + 2\sigma_3)/3 - P_p$) and differential stress Q ($= \sigma_1 - \sigma_3$). At a given value of P the onset of shear-enhanced compaction occurs in a dry sandstone sample at a stress value Q that is markedly higher than that in a saturated sample.

Wong et al. [1997] suggested that the grain crushing pressure P^* is a quantitative measure of the brittleness of a sandstone. It can be seen from Table 2 and Figure 8 that for the same sandstone the value of P^* of a nominally dry sample is higher than that for the saturated sample. The dry sandstone is therefore considered to be more brittle than the saturated sandstone in that the brittle-ductile transition occurs at a somewhat higher effective pressure and that the postpeak deformation tends to be more unstable in the brittle faulting regime.

Figure 7b also shows that the porosity change behavior at effective pressures of 10 MPa was such that the compaction decelerated in comparison to the hydrostat beyond critical stress states marked as C'. This implies that at stress levels beyond C' the deviatoric stress field induced the pore space to dilate. This phenomenon of dilatancy is commonly observed in the brittle fracture regime [*Brace*, 1978; *Wong et al.*, 1997]. Values of C' were determined for all samples that failed by brittle faulting (Table 1).

3. Fracture Mechanics Analyses of Water Weakening

Brittle faulting and cataclastic flow are two fundamentally different failure modes. However, since they both involve microcracking as well as acoustic emissions, in both cases the evolution of internal damage must be strongly influenced by the grain-scale fracture mechanisms that control the nucleation and propagation of cracks. According to the *Griffith* [1920] theory the mechanics of fracture in an ideally brittle solid is governed by the specific surface energy γ, such that equilibrium propagation of a crack occurs if the strain energy release rate G attains the critical value (also called the fracture energy) $G_c = 2\gamma$. Equivalently, this condition can be expressed in terms of the stress intensity factors [*Irwin*, 1958]. In an elastic solid (with Young's modulus E and Poisson's ratio ν), extensile crack growth (in plane strain condition) occurs if the stress intensity factor K_I attains the critical value such that K_{IC} such that

$$G_c = \frac{(1-\nu^2)}{E} K_{IC}^2 = 2\gamma . \qquad (1a)$$

One of the earliest theories of chemistry in brittle fracture was that of *Orowan* [1944], who proposed that the environmental

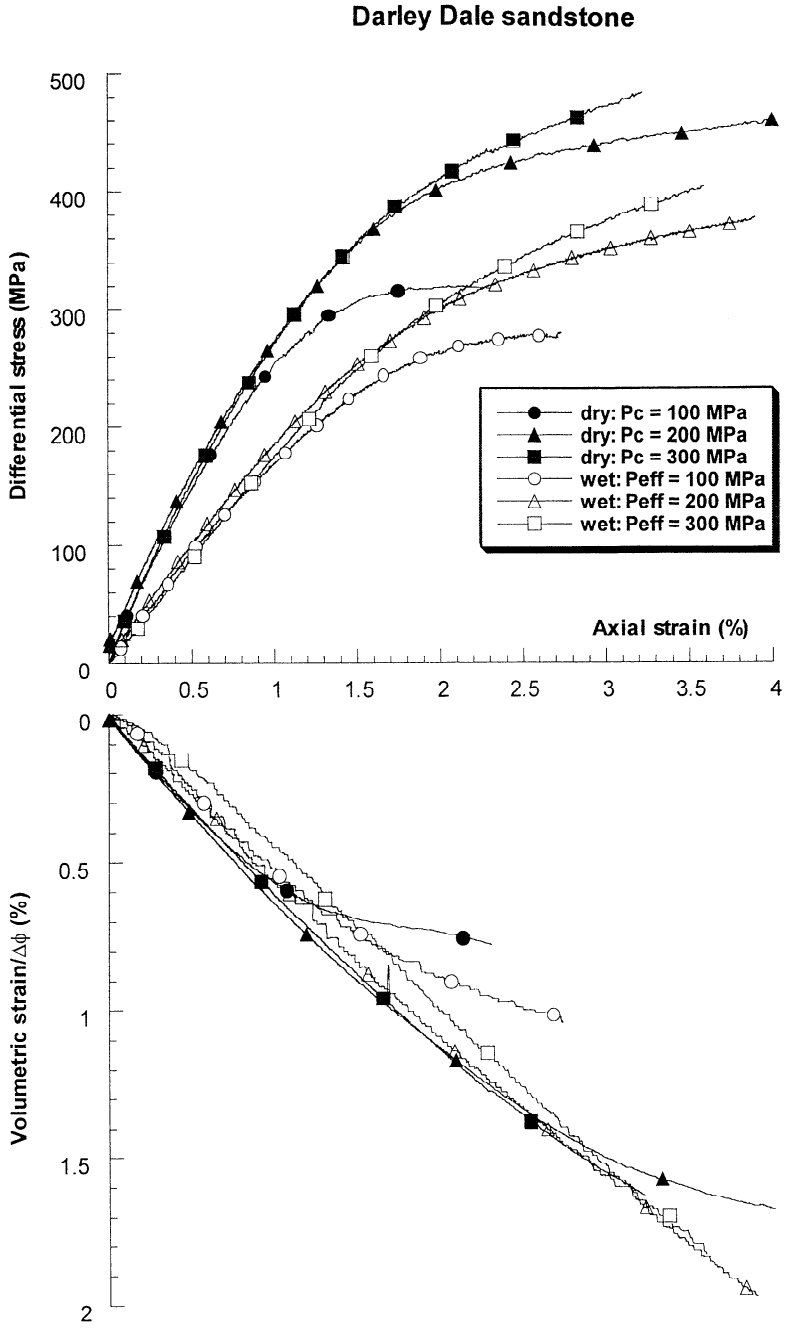

Figure 4. Mechanical data for Darley Dale sandstone samples deformed in the cataclastic flow regime. Differential stress and volumetric strain (or porosity change) were plotted versus axial strain. The open symbols are for water-saturated samples, and the solid symbols are for the nominally dry samples.

molecules lower the interface energy on entering the crack interface and adsorbing onto the walls in the cohesion/adhesion zone. As elaborated by *Lawn* [1993], Orowan's generalization of the Griffith-Irwin equilibrium concept is best described in terms of the Dupré work of adhesion [*Israelachvili*, 1991]. While the decohesion of a solid body in vacuum is characterized by the specific surface energy γ, the separation of two solid half bodies (B) in a fluid environment (E) is characterized by the solid-fluid interface energy γ', that is, the energy to form one unit area interface (B-E) relative to the initial cohesion state (B-B). For the environmentally susceptible system, equilibrium propagation of a tensile crack occurs if the strain energy release rate (or stress intensity factor) attains the critical value G_c' (or K_{IC}') such that

$$G_c' = \frac{(1-\nu^2)}{E} K_{IC}'^2 = 2\gamma' . \quad (1b)$$

If $\gamma' < \gamma$, then adsorption occurs and the cohesion of the solid is lowered by the environmental interaction, with corresponding reduction in strength that is related to the ratio

$$\lambda = \gamma'/\gamma = (K_{IC}'/K_{IC})^2 . \quad (2)$$

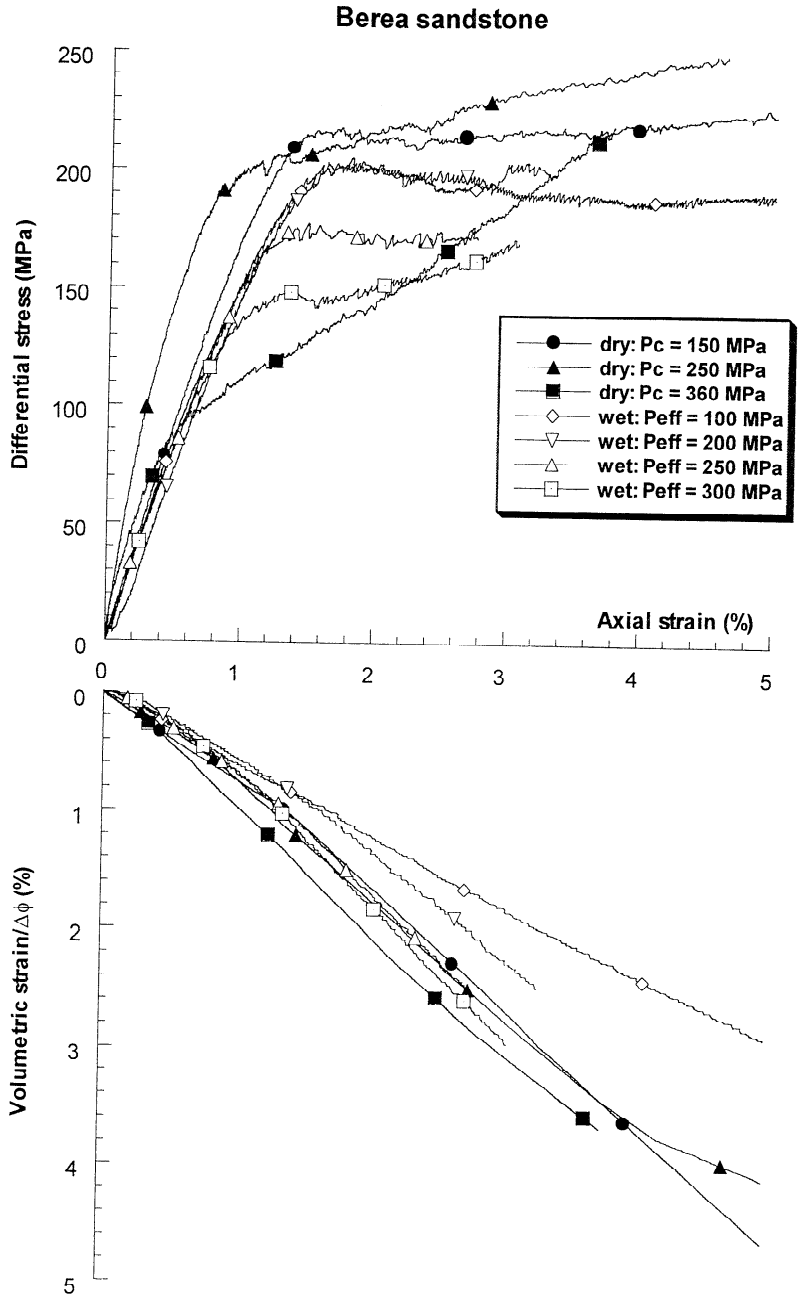

Figure 5. Mechanical data for Berea sandstone samples deformed in the cataclastic flow regime. Differential stress and volumetric strain (or porosity change) were plotted versus axial strain. The open symbols are for water-saturated samples, and the solid symbols are for the nominally dry samples.

The energetics of adsorption are such that the ratio decreases with increasing temperature and activity of the environmental species [*Lawn*, 1993].

Since Orowan's generalization of the Griffith theory is still based on the first law of thermodynamics, it is valid only for a crack system that is perturbed incrementally from equilibrium and therefore cannot be used to describe the kinetics of crack growth. Using the more general framework of irreversible thermodynamics, *Rice* [1978] demonstrated that for crack speeds v that are small relative to sonic speeds, the strain energy release rate G and specific surface energy γ' in an ideally brittle solid should be constrained by the inequality

$$(G-2\gamma')v \geq 0 . \quad (3)$$

The inequality implies that there exists a steady state relation between v and G for the forward and backward propagation (i.e., extension and healing) of a crack in a chemically active environment, with a threshold $v=0$ at $G=2\gamma'$ [*Lawn*, 1993].

Such chemical effects have not been explicitly accounted for in most micromechanical modeling of compressive failure. To interpret our laboratory data on water-weakening effects in the brittle faulting and cataclastic flow regimes, we have modified the "sliding wing crack" [*Horii and Nemat-Nasser*, 1986; *Ashby and Sammis*, 1990; *Kemeny and Cook*, 1991]

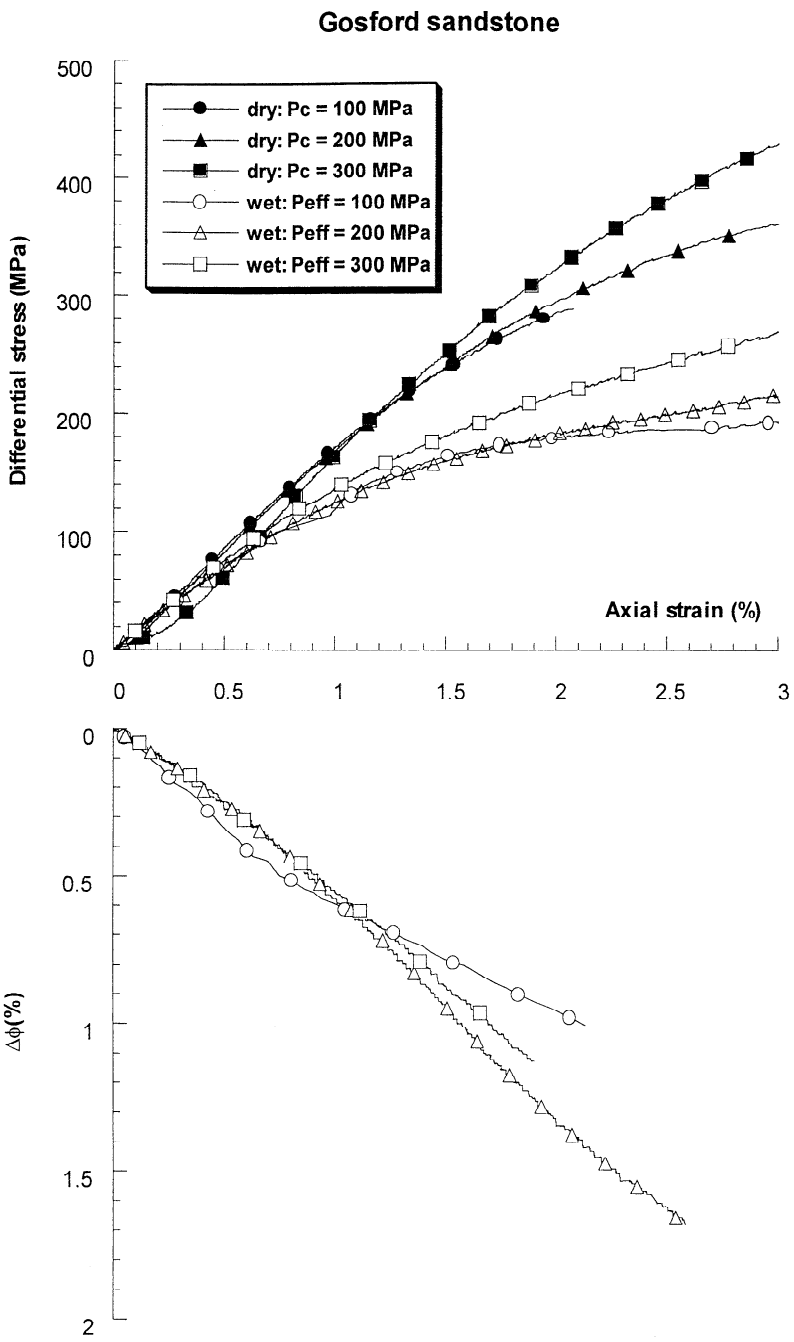

Figure 6. Mechanical data for Gosford sandstone samples deformed in the cataclastic flow regime. Differential stress and porosity change were plotted versus axial strain. The open symbols are for water-saturated samples, and the solid symbols are for the nominally dry samples.

and Hertzian fracture [*Zhang et al.*, 1990b] models by incorporating the chemically induced effects, specifically the reductions of fracture energy and toughness as characterized by the ratio λ defined in (2).

3.1. Cataclastic Flow Regime: Hertzian Fracture Model

Microstructural observations of deformed samples have documented that grain crushing and pore collapse are the dominant micromechanical processes in the compactive cataclastic flow regime [*Zhang et al.*, 1990b; *Menéndez et al.*, 1996; *Wu et al.*, 2000]. The stress-induced microcracks radiate from grain contacts in patterns reminiscent of extensile indentation fractures, usually referred to as Hertzian fracture. *Zhang et al.* [1990b] proposed a micromechanical model for such cataclastic deformation, in which the pore space and the grain geometry are represented by a random packing of several distinct sizes of spherical particles in elastic contact. Identifying the onset of grain crushing with the initiation of Hertzian fracture, they used elastic contact theory and linear elastic fracture mechanics to arrive at the following expression for the critical pressure P^* for the onset of grain crushing under hydrostatic loading:

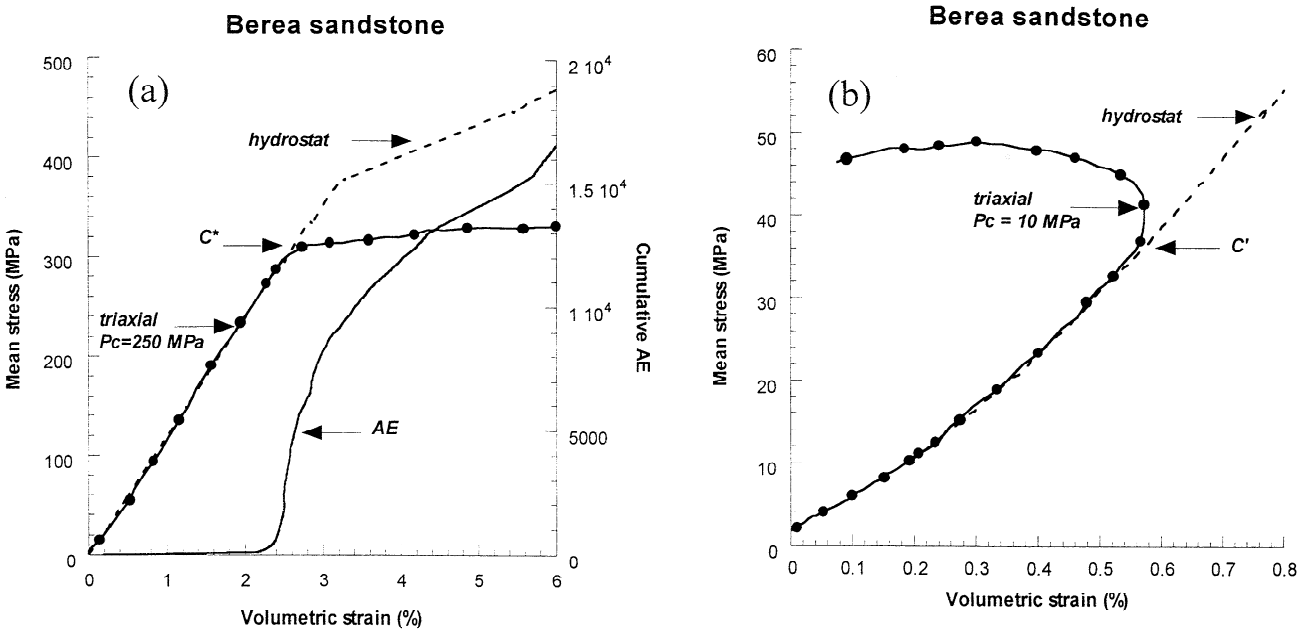

Figure 7. Examples of the determination of (a) the onset of shear-enhanced compaction C^* and (b) onset of dilatancy C' for dry Berea sandstone experiments at confining pressures of 250 MPa and 10 MPa, respectively. The hydrostat is shown as dashed curves. Acoustic emission data for the triaxial experiment are also included in Figure 7a. Volumetric changes corresponding to pressurization are included in both graphics.

$$P^*_{\text{dry}} = 2.2\,\frac{(1-\nu^2)^2}{E^2(1-2\nu)^3}\,\frac{K_{IC}{}^3}{(\phi c)^{3/2}}, \tag{4a}$$

where ϕ is the porosity and c is the length of preexisting crack at the proximity of the grain contact (Figure 9a). Since environmental interaction is not expected to have insignificant impact on the elastic moduli, initial crack length, or porosity, the critical pressure P^*_{wet} in a saturated sample is expected to have a lower value that arises primarily from environmentally induced reduction of the fracture toughness

$$P^*_{\text{wet}} = 2.2\,\frac{(1-\nu^2)^2}{E^2(1-2\nu)^3}\,\frac{K'_{IC}{}^3}{(\phi c)^{3/2}}. \tag{4b}$$

This implies that in the Hertzian fracture model the water-weakening effect on grain crushing is related to the ratio λ in the following manner:

$$\frac{P^*_{\text{wet}}}{P^*_{\text{dry}}} = \left(\frac{K'_{IC}}{K_{IC}}\right)^3 = \left(\frac{\gamma'}{\gamma}\right)^{3/2} = \lambda^{3/2}. \tag{5}$$

Using this approach, our hydrostatic data on grain crushing pressure (Table 2) can be used to infer λ. The values of λ so inferred are compiled in Table 3.

For nonhydrostatic loading, *Wong et al.* [1997] concluded that the initial yield stresses at the onset of shear-enhanced compaction can be described in the stress space by an elliptic envelope that scales with the grain crushing pressure P^*. The compactive yield envelope can be expressed in terms of the following parametric equations for the effective mean stress and differential stress:

$$P = P^*\left[\xi + (1-\xi)\cos\theta\right] \tag{6a}$$

$$Q = P^*\delta\sin\theta, \tag{6b}$$

where θ ranges from 0 to $\pi/2$. A change in symbol should be noted: the parameter ξ here is the same as parameter γ of *Wong et al.* [1997]. The brittle-ductile transition occurs at the stress state corresponding to $P=\xi P^*$ and $P=\delta P^*$. We used this transition condition to determine the parameters ξ and δ for both the saturated and nominally dry sandstone samples (Table 3). Together with laboratory data for P^*_{wet} and P^*_{dry}, the parameters for (6) are completely specified, and (6) can be used to map out the initial yield envelope. As shown in Figure 10, both the saturated and nominally dry data (for samples that failed in the cataclastic flow and transitional regimes) are in reasonable agreement with the elliptic envelopes.

3.2. Brittle Faulting Regime: Sliding Wing Crack Model

Dilatancy in brittle rock has been observed to arise from intragranular and intergranular cracking with a preferred orientation parallel to the maximum principal stress σ_1. In the strain softening stage, microcracking and acoustic emission activity begin to be localized along a macroscopic shear band [*Tapponier and Brace*, 1976; *Wong*, 1982; *Lockner et al.*, 1992; *Menéndez et al.*, 1996; *Wu et al.*, 2000]. A conceptual model widely used to analyze such micromechanical processes is the sliding wing crack [e.g., *Horii and Nemat-Nasser*, 1986; *Ashby and Sammis*, 1990; *Kemeny and Cook*, 1991; *Baud et al.*, 1996; *Baud and Reuschlé*, 1997]. The model considers the growth of "wing cracks" that initiate from tensile stress concentration at the tips of preexisting

Table 2. Mechanical Data for Sandstone Samples That Failed by Compactive Cataclastic Flow

Effective Pressure $\sigma_3 - P_p$, MPa	Dry C^* Effective Mean Stress P, MPa	Dry C^* Differential Stress Q, MPa	Wet C^* Effective Mean Stress P, MPa	Wet C^* Differential Stress Q, MPa	Weakening [a] Q(Wet)/Q(Dry)
		Darley Dale			
100	205	315	185	261	0.74
150	-	-	245	285	-
200	314	342	290	263	0.71
300	395	284	350	153	0.70
P*	470	0	380	0	-
		Berea			
100	-	-	165	196	-
150	220	208	-	-	-
200	-	-	260	178	-
250	310	180	301	151	0.83
300	-	-	341	122	-
360	388	72	-	-	-
P*	400	0	380	0	-
		Gosford			
100	200	300	158	174	0.69
200	305	315	254	160	0.66
300	385	255	323	70	0.47
P*	440	0	335	0	-
		Boise			
5	-	-	14	27	-
6	23	48	-	-	-
10	28	51	20	30	-
15	-	-	25	30	-
20	-	-	30	30	-
30	-	-	37	21	-
35	50	44	39	12	0.31
P*	62	0	44	0	-

[a] Calculated ratio is for differential stresses of saturated and dry samples that were attained at axial strains of 1.5%.

cracks undergoing frictional slip. The fracture mechanics is such that increasing the stress causes the wing crack to propagate along a curved path and ultimately to reach a stable orientation parallel to the direction of σ_1 (Figure 9b). With the accumulation of such anisotropic cracking distributed throughout the rock, the damage will ultimately attain a critical state at which the multiplicity of cracks coalesce to develop a shear band.

The sliding wing crack model considers sources of tensile stress concentration that are located at the tips of preexisting cracks (with initial length $2c$ and oriented at angle γ to σ_1). The applied stresses induce a shear traction on the crack plane, and if this resolved shear traction is sufficiently high to overcome the frictional resistance along the closed crack, frictional slip results in tensile stress concentrations at the two tips which may induce wing cracks to nucleate and extend out of the initial plane of the main sliding crack. In the Griffith-Irwin framework the driving force is characterized by the stress intensity factor K_I at the tip of the putative wing crack. With increased loading, it will attain the critical value K_{IC}, at which point a wing crack nucleates and propagates along a curved path to ultimately reach a stable orientation parallel to the direction of σ_1.

If the onset of dilatancy C' is identified with the initiation of wing cracks and if the rock is assumed to contain randomly oriented cracks, then the wing cracks should first nucleate from those sliding cracks oriented at $\gamma = 1/2\tan^{-1}(1/\mu)$, where μ is the frictional coefficient. The principal stresses at the onset of dilatancy are given by [*Cotterell and Rice*, 1980; *Horii and Nemat-Nasser*, 1986; *Ashby and Sammis*, 1990]

$$\sigma_1 = \frac{\sqrt{1+\mu^2}+\mu}{\sqrt{1+\mu^2}-\mu}\sigma_3 + \frac{\sqrt{3}}{\sqrt{1+\mu^2}-\mu}\frac{K_{IC}}{\sqrt{\pi c}}. \quad (7)$$

As the density of wing cracks increases, they coalesce to form a macroscopic shear band in the strain-softening stage. To analyze the peak stress data, we adopted *Ashby and Sammis'* [1990] two-dimensional model for mathematical convenience. The key damage parameter in this model is the crack density $D = \pi(l + c\cos\gamma)^2 N_A$, where ℓ is the length of the wing crack and N_A is the number of sliding cracks per unit area initially present. Before wing cracks nucleate, the length $l = 0$ and therefore the initial damage is given by $D_o = \pi(c\cos\gamma)^2 N_A$. With the progressive development of dilatancy, the principal stresses evolve with damage in accordance with equation (17) of *Ashby and Sammis* [1990]:

$$\sigma_1 = \left[C_1 + \frac{C_4\left[\sqrt{D/D_o}-1\right]}{1+\sqrt{\pi D_o}\left(\sqrt{D/D_o}-1\right)/\left(1-\sqrt{D}\right)} \right]\sigma_3$$

$$+ \frac{\sqrt{D/D_o}-1+0.1/\cos\gamma}{1+\sqrt{\pi D_o}\left(\sqrt{D/D_o}-1\right)/\left(1-\sqrt{D}\right)} \frac{C_4}{\sqrt{\cos\gamma}} \frac{K_{IC}}{\sqrt{\pi c}} \quad (8)$$

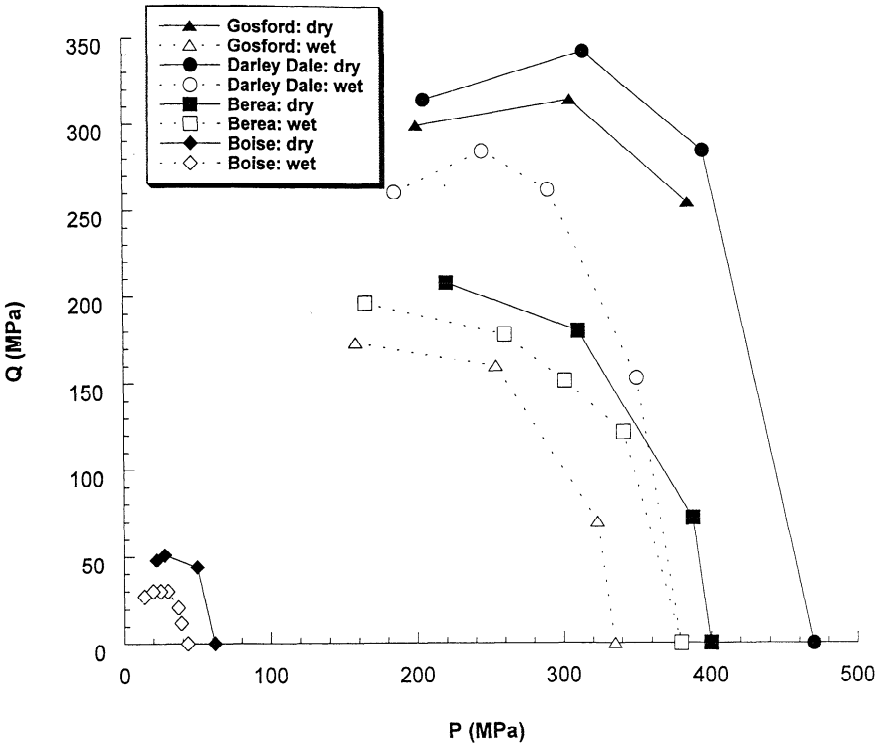

Figure 8. Summary of mechanical data for onset of shear-enhanced compaction in four sandstones. Stress state C^* is shown in the P (effective mean stress) and Q (differential stress) space. The open symbols are for water saturated samples and the close symbols for the nominally dry samples.

where $C_1 = (\sqrt{1+\mu^2} + \mu)/(\sqrt{1+\mu^2} - \mu)$

and $C_4 = \sqrt{30}\cos\gamma/(\sqrt{1+\mu^2} - \mu)$.

If the parameters D_o, $K_{IC}/(\pi c)^{1/2}$, and μ have been specified, then the evolution of the principal stress σ_1 as a function of damage D at a fixed confining stress σ_3 can be calculated using (8). In the brittle faulting regime the stress attains a peak beyond which instability sets in. Repeating the calculation for different values of fixed σ_3 allows one to map out the brittle failure envelope in the principal stress space.

To a first approximation this failure envelope for the wing crack model [*Horii and Nemat-Nasser*, 1986; *Ashby and Sammis*, 1990; *Fredrich et al.*, 1990; *Kemeny and Cook*, 1991] can be described by a linear relation

$$\sigma_1 = A(\mu, D_o)\,\sigma_3 + B(\mu, D_o)\,K_{IC}/\sqrt{\pi c}\,. \qquad (9)$$

For a given rock the initial damage D_o can be considered to be identical in both dry and saturated conditions. As discussed above, the fracture toughness in vacuum may be significantly higher than that in the presence of water due to environmental interaction. Along the fluid-solid interface, the friction coefficient may also be reduced by lubrication due to the fluid. To account for these differences, we modified (7) by replacing the fracture toughness and friction coefficient with values K'_{IC} and μ' that are considered to be appropriate for a fluid-saturated rock:

$$\sigma_1 = \frac{\sqrt{1+\mu'^2} + \mu'}{\sqrt{1+\mu'^2} - \mu'}\sigma_3 + \frac{\sqrt{3}}{\sqrt{1+\mu'^2} - \mu'}\frac{K'_{IC}}{\sqrt{\pi c}}. \qquad (10a)$$

Equation (10a) specifies the condition for the onset of dilatancy in a fluid-saturated rock. An analogous modification was made in (8), which was then used to calculate the linear envelope for brittle fracture in the water-saturated rock

$$\sigma_1 = A'(\mu', D_o)\,\sigma_3 + B'(\mu', D_o)\,K'_{IC}/\sqrt{\pi c}\,. \qquad (10b)$$

Following previous studies [*Horii and Nemat-Nasser*, 1986; *Ashby and Sammis*, 1990; *Fredrich et al.*, 1990], a value of $\gamma = 45^o$ was assumed in (8) for all our calculations for both nominally dry and saturated cases. It should be noted that a particularly simple result is obtained if the presence of water has negligible effect on the friction coefficient so that $\mu \approx \mu'$. It can then be seen from (9) and (10b) that for this end-member the ratio of the unconfined compressive strength of a water-saturated sample (σ_{wet}) to that of a dry sample (σ_{dry}) is simply given by

$$\sigma_{wet}/\sigma_{dry} = K'_{IC}/K_{IC} = \sqrt{\lambda} = (P^*_{wet}/P^*_{dry})^{1/3} \qquad (11)$$

If the triaxial compression data for a water-saturated rock follow the linear trends described by (10a) and (10b), then the slopes and intercepts of the two sets of stress data at the onset of dilatancy and peak provide four constraints for inferring the three parameters D_o, $K'_{IC}/(\pi c)^{1/2}$, and μ'. Similarly, if the

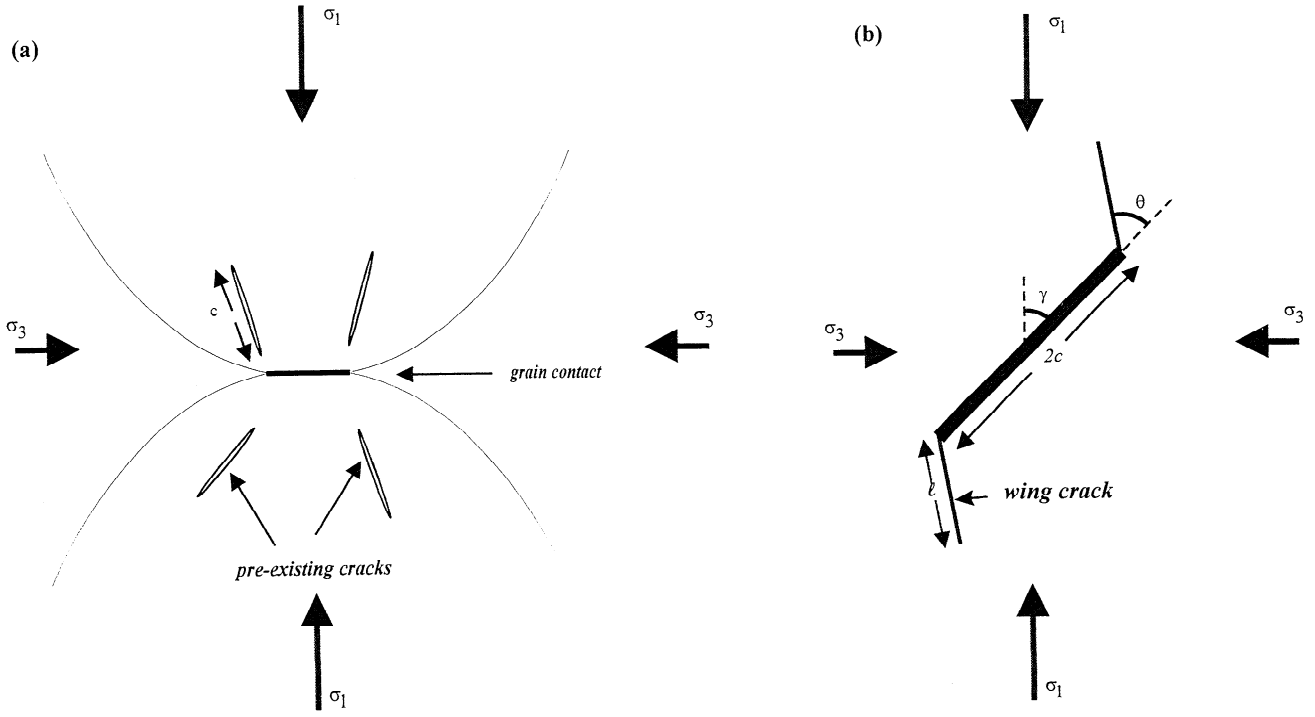

Figure 9. Schematic diagrams illustrating the micromechanical models: (a) Herztian fracture model for the onset of grain crushing in the compactive cataclastic flow regime; and (b) sliding wing crack model for the development of dilatancy and instability in the brittle faulting regime.

data for a dry rock follow the linear trends described by equations (8) and (10), then the two sets of stress data at the onset of dilatancy and peak also provide four constraints for inferring the two parameters $K_{IC}/(\pi c)^{1/2}$ and μ (with the initial damage D_o fixed at the value inferred for the saturated samples). Our mechanical data are sufficiently comprehensive to provide the eight constraints for inferring the five parameters $K_{IC}/(\pi c)^{1/2}$, $K'_{IC}/(\pi c)^{1/2}$, μ, μ', and D_o for each of the four sandstones. The fit of our data to the linear envelopes are shown in Figure 11, and the inferred values for these parameters (as well as for λ) are compiled in Table 4. We could not conduct this analysis on Gosford sandstone due to the small number of samples that we had in the brittle faulting regime.

4. Discussion

In this study, we have systematically studied the chemical influence of water on the mechanical properties of four sandstones with porosities ranging from 11% to 35%. The pressure ranges were sufficiently wide that the transitions from brittle faulting to compactive cataclastic flow ware observed in Darley Dale and Berea sandstones. For these two rocks the critical stresses at the onset of shear-enhanced compaction and dilatancy, as well as the brittle strength were determined for nominally dry and saturated samples under comparable effective pressure conditions. For Gosford and Boise sandstones we were able to determine only the critical stresses at the onset of shear-enhanced compaction. In each sandstone the critical stresses were observed to decrease in the presence of water. The compactive yield strengths in the saturated samples were lower than those in the dry samples deformed under comparable pressure conditions by 20% to 70%. The reductions of brittle strength in the presence of water ranged from 5% to 17%. While water-weakening effect varies widely among the sandstones, the weakening effects in the brittle faulting and cataclastic flow regimes are correlated in that the sandstone with relatively large reduction of brittle strength was also observed to have relatively large reduction of compactive yield stress. The water-weakening effects were most and least significant in the Gosford and Berea sandstones, respectively.

4.1. Fracture Energy, Water Weakening and Compactive Cataclastic Flow

With reference to the Hertzian fracture model, we interpreted the water-weakening effect in the compactive cataclastic flow regime as primarily due to the lowering of the fracture energy in the presence of water [*Orowan*, 1944; *Lawn*, 1993]. We characterized the water-weakening effect on the fracture energy by the parameter λ as defined in (2). Our data sets for the onset of shear-enhanced compaction in nominally dry and saturated sandstone samples can each be described by an elliptical envelope (equation (6)) that scales with the grain crushing pressure (Figure 10). Therefore the reduction of this critical pressure in the presence of water characterizes the overall water-weakening effect in the cataclastic flow regime. According to (5) the reduction in grain crushing pressure can be used to directly infer the fracture energy reduction λ.

Our analysis (Table 3) shows that the water-weakening effect in the cataclastic flow regime can be explained by comparable values of λ (that range from 0.83 to 0.89) in the Darley Dale, Gosford, and Boise sandstones, while the water-

Table 3. Compactive Yield and Weakening Parameters Inferred From Sandstone Data

Sandstone	ξ (Dry)	δ (Dry)	ξ (Wet)	δ (Wet)	λ
Gosford	0.60	0.74	0.57	0.53	0.83
Darley Dale	0.61	0.74	0.57	0.74	0.87
Berea	0.57	0.52	0.55	0.51	0.97
Boise	0.55	0.85	0.55	0.72	0.79

weakening effect is almost negligible in Berea sandstone (with $\lambda = 0.97$). These relatively small reductions in fracture energy due to the presence of water are in agreement with limited fracture mechanics data for silicate minerals and rocks [*Meredith and Atkinson*, 1983; *Atkinson and Meredith*, 1987; *Lajtai et al.*, 1987].

Zhang et al. [1990b] have concluded that if (4) is supplemented by the plausible assumption that the preexisting crack length c scales with the grain radius R, then it describes quite well the dependence of grain crushing pressure on porosity and grain size. If we use (5) to explicitly account for the additional effect of water weakening, then the relation of *Zhang et al.* [1990b] can be modified to give

$$P^* \propto \left(\frac{\lambda}{\phi R}\right)^{3/2}, \tag{12}$$

where the ratio λ has a value of unity in vacuum and a value less than one for a sandstone saturated with fluid. According to the above, an environmentally induced reduction of surface energy of 10% has the same consequence on the grain

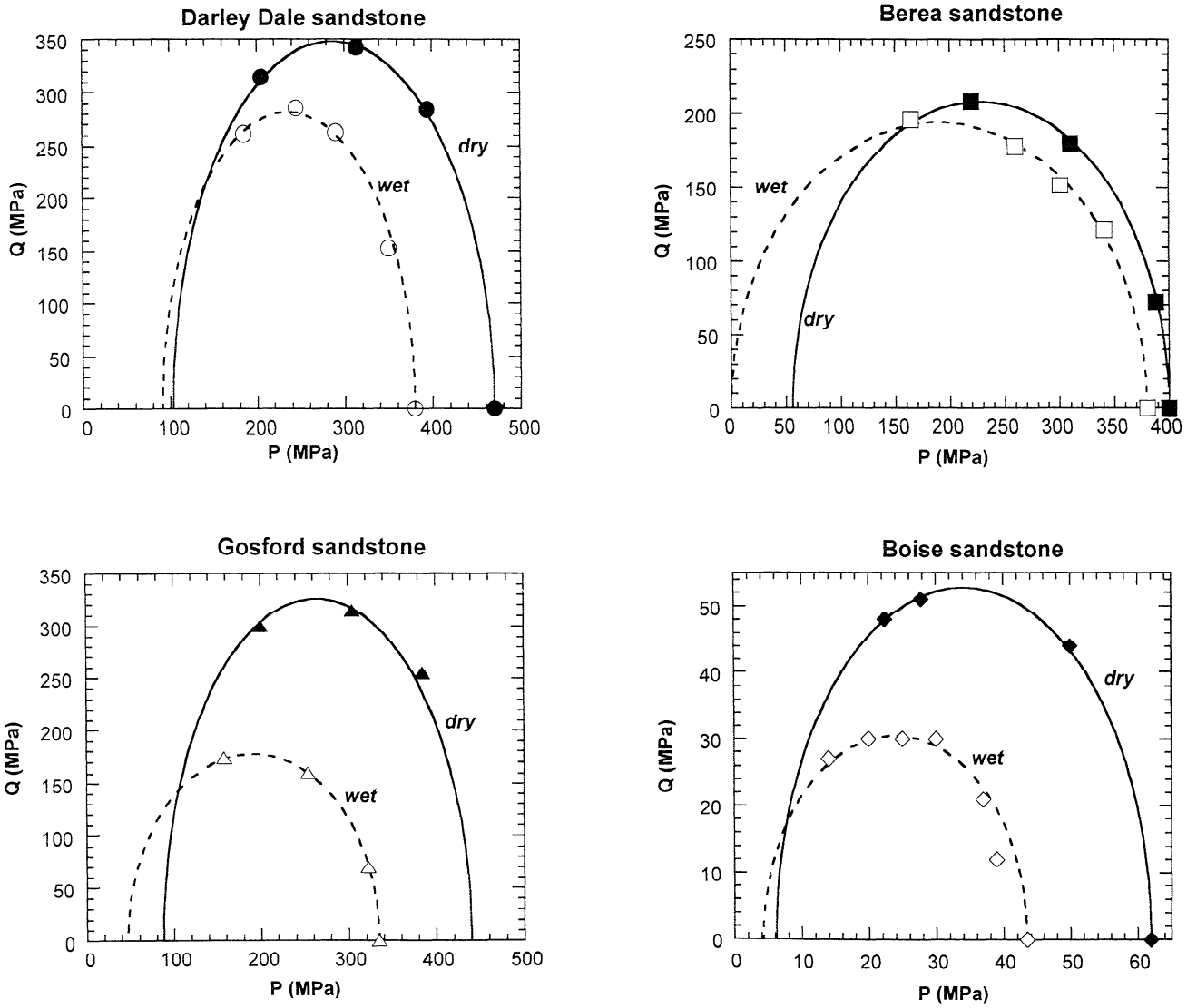

Figure 10. Elliptical compactive yield envelopes (equation (6)) that fit the data for the onset of shear-enhanced compaction for the four sandstones in dry and wet conditions. The parameters of the envelopes are given in Table 3.

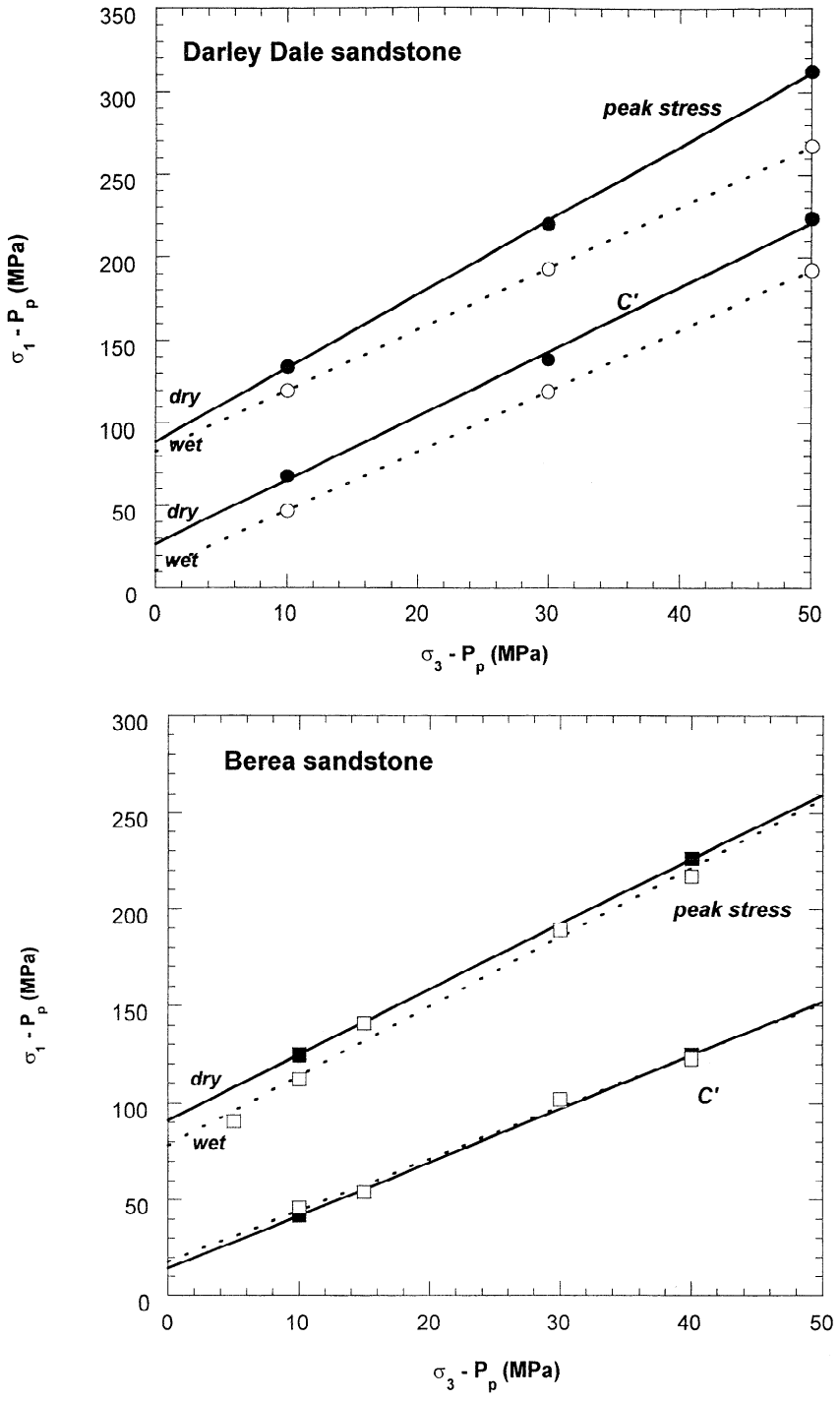

Figure 11. Comparison of the peak stress and C' data and theoretical predictions of *Ashby and Sammis'* [1990] model using damage and fracture mechanics parameters compiled in Table 4.

crushing pressure as an increase of the grain size by 10% (or comparable increase in porosity).

4.2. Fracture Energy, Friction Coefficient, and Water Weakening of Brittle Strength

In the brittle faulting regime the sliding wing crack model was used to interpret our data on the onset of dilatancy and peak stress. According to our analysis the brittle strength may be lowered in the presence of water due to reductions in the fracture energy as well as the friction coefficient. If the water-weakening effect on the friction coefficient is relatively small, then (11) establishes a simple relation among the reductions in unconfined compressive strength, grain crushing pressure, fracture energy, and fracture toughness. To a certain extent, our data for the Berea and Darley Dale sandstone (Tables 3 and 4) agree with this limiting case. For the Lac du Bonnet granite, *Lajtai et al.* [1987] directly measured the unconfined compressive strength and fracture toughness of nominally dry

Table 4. Wing Crack and Water-Weakening Parameters Inferred From Sandstone Data

Rock	μ (Dry)	μ' (Wet)	μ'/μ	D_o	$K_{IC}/(\pi c)^{1/2}$ (Dry), MPa	$K'_{IC}/(\pi c)^{1/2}$ (Wet), MPa	$\lambda=(K'_{IC}/K_{IC})^2$
Darley Dale	0.74	0.66	0.89	0.44	25.0	27.0	0.86
Berea	0.56	0.51	0.91	0.3	29.0	28.5	0.97

and saturated samples. Their data show that both the unconfined strength and fracture toughness of the granite were reduced by ~10% in the presence of water, in good agreement with (11) with $\lambda \sim 0.8$.

However, the pressure dependences of the brittle strength of the nominally dry and saturated samples of the same sandstone can also be quite different. In these cases the water-weakening phenomena in the brittle faulting regime cannot be explained solely in terms of the reduction of fracture energy. Our data for the onset of dilatancy and peak stress indicate that the friction coefficient can be lowered by ~10% in the presence of water (Table 4), which also contributes to the strength reduction. After accounting for the differences in friction coefficient the weakening effects of water on the compactive yield stress and brittle strength in all our sandstone samples can be consistently explained in a fracture mechanics framework using almost identical values of λ.

It should be noted that although our estimates of D_o, K_{IC}, and μ are by no means unique, the experimental data do provide rather tight constraints. According to (7) and (10a) the slope of the C' data depends only μ. Our experience with this type of analysis using the wing crack model shows that D_o and μ control the slope A (or A') of the peak stress data (as given by (9) or (10b)), and our estimation of D_o and μ primarily hinges on the slopes of the C' and peak stress data. Our experience with this type of analysis also shows that D_o and $K_{IC}/(\pi c)^{1/2}$ (or $K'_{IC}/(\pi c)^{1/2}$) control the intercept B (or B') in (9) (or (10b)). With D_o inferred from the slopes of the dry and saturated rock data, $K_{IC}/(\pi c)^{1/2}$ (or $K'_{IC}/(\pi c)^{1/2}$) can be adjusted so (9) (or (10b)) provide intercepts in agreement with the peak stress data. In practice, the intercepts of the C' data carried the least weight in our estimation scheme even though it is relatively straight forward to use (7) (or (10a)) to infer $K_{IC}/(\pi c)^{1/2}$ (or $K'_{IC}/(\pi c)^{1/2}$). Experimental data on the onset of dilatancy are such that they are not as reproducible as peak stress data, and consequently, significant uncertainty is associated with the intercept value inferred from C' data. Although values of $K'_{IC}/(\pi c)^{1/2}$ inferred directly from C' data [*Wu et al.*, 2000] are significantly lower than those compiled in Table 4, we consider our estimates on the basis of peak stress data to be more reliable.

The inferred values for friction coefficients fall in typical ranges of experimental measurements for quartz and feldspar [*Horn and Deere*, 1962] and are comparable to values inferred for other silicate rocks using the wing crack model [*Ashby and Sammis*, 1990; *Wu et al.*, 2000]. Our estimates of $K_{IC}/(\pi c)^{1/2}$ (or $K'_{IC}/(\pi c)^{1/2}$) are considered to be reasonable. If we assume values of $2c$ equal to the average grain sizes of Berea and Darley Dale sandstone, then K_{IC} and K'_{IC} are estimated to be ~ 0.6 MPa $m^{1/2}$ that is comparable to experimental measurements for quartz [*Atkinson and Meredith*, 1987].

The initial damage D_o was found to be larger in Darley Dale sandstone than in Berea sandstone (Table 4). In comparison, *Menéndez et al.* [1996] and *Wu et al.* [2000] in recent microstructural studies observed that the density of preexisting crack (as characterized by linear intercept measurement) in Berea sandstone is about twice that in Darley Dale sandstone. However, such a quantitative comparison should not be taken at face values since the damage parameter D_o depends on the square (or cube) of crack length in a two- (or three-) dimensional model, whereas the microstructural measurement of linear intercept density is linearly related to the crack length [*Wong*, 1985]. The D_o values in Table 4 and microstructural data are not in disagreement if the crack length distribution of Darley Dale sandstone is skewed more toward the longer cracks. *Ashby and Sammis* [1990] inferred smaller values of D_o (between 0.01 and 0.2) for several compact rocks. For the Bunt sandstone (with an initial porosity of 15%) they inferred a D_o value of 0.15.

4.3. Mechanisms and Kinetics of Water Weakening

Our analysis indicates that the reductions of fracture energy and friction coefficient due to the presence of water are positively correlated (Tables 3 and 4), implying that the operative mechanisms are effective on both crack propagation and frictional sliding. The weakening effect is more pronounced in sandstone with larger fractions of altered feldspar and clay minerals. Notwithstanding our success in analyzing the water-weakening effects in both brittle faulting and cataclastic flow regimes on the basis of equilibrium concepts of fracture mechanics, we have not identified the specific mechanisms by which the fracture energy is reduced or addressed the question as to why the reduction effect λ varies widely among different sandstones. This would require a quantitative analysis of the reaction kinetics that is beyond the scope of the present study.

As a pilot study, we have also conducted some tests on the rate dependence of the water-weakening effect. Figure 12a presents the results for saturated samples of Darley Dale samples at 200 MPa effective pressure at three different strain rates ranging from 2×10^{-6} to 5×10^{-5} s^{-1}. It can be seen that rate dependence was not appreciable. Similar results were obtained in the brittle regime. This conclusion is consistent with creep tests on Darley Dale sandstone [*Baud and Meredith*, 1997]. However, it should also be noted that in tests that lasted for several days (in which the loading ram was locked and sample allowed to relax at different stages) the mechanical data do indicate appreciable dependence on rate [*Zhu and Wong*, 1997]. Observation of stress relaxation would probably allow sampling a much larger range of instantaneous strain rate [*Rutter and Mainprice*, 1978].

Even though it is not specified in Rice's kinetic theorem (equation (3)), several relations between the crack speed v and strain energy release rate G (or stress intensity factor K) have been proposed. On purely empirical grounds, the simple power law relation $v \propto K^n$ has been used [*Charles*, 1958;

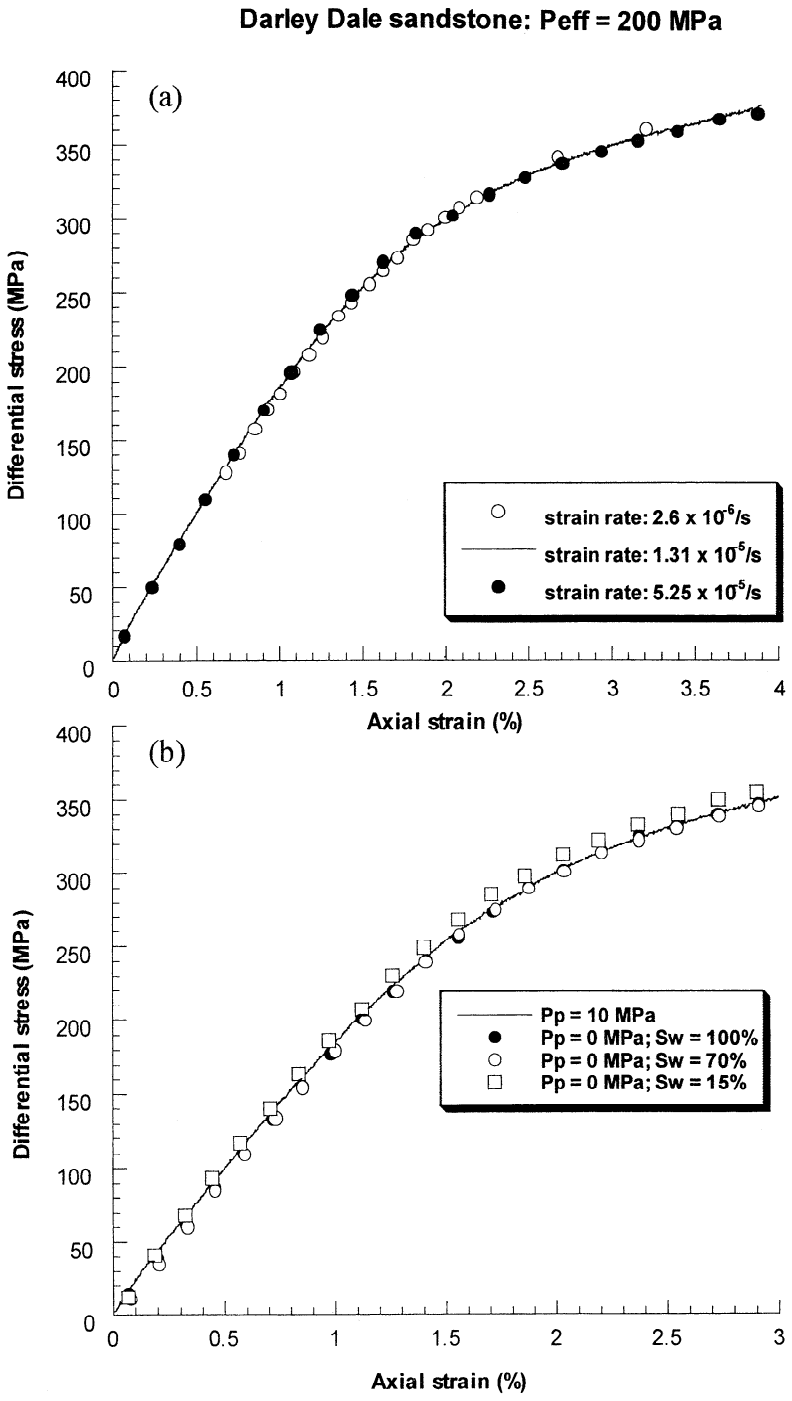

Figure 12. Differential stress versus axial strain for Darley Dale sandstone samples deformed at effective pressure of 200 MPa. (a) Mechanical data at the same pore pressure of 10 MPa and three different strain rates (2.6×10^{-6} s^{-1}, 1.3×10^{-5} s^{-1}, 5.25×10^{-5} s^{-1}) indicate insignificant rate sensitivity. (b) Effect of pore pressure and water saturation. Mechanical data for saturated samples at ambient and 10 MPa pore pressure were identical, but data for samples at different saturation degrees (S_W) indicate slight strengthening in the initially unsaturated samples, possibly due to capillary effects.

Atkinson and Meredith, 1987]. If crack growth is modeled as being due to adsorption-induced reduction in bond strength, with the crack speed controlled by the rate of adsorption at the crack tip, then it obeys an exponential relation of the form $v \propto \exp(bK)$ [*Charles and Hillig*, 1962; *Wiederhorn and Bolz*, 1970]. A further relationship, derived from the classical theory of rate processes [*Lawn*, 1975] gives an exponential relation of the form $v \propto \exp(\alpha G) \propto \exp(\beta K^2)$. In each case, the temperature dependence can be introduced as an Arrhenius factor in the proportionality "constant." However, these kinetic models can be used in the present context only if the crack speed v can be related to the macroscopic strain

rate. This requires systematic investigation of the creep behavior at different temperatures or in the presence of fluids of various chemistry.

Our experiments and micromechanical models apply only to cases when the pore space is fully saturated. However, there are many geophysical and geotechnical applications in which the pore space may be partially saturated. In such cases, the mechanical behavior may be influenced by capillary actions [*Lawn*, 1993]. We have also conducted preliminary tests to study this phenomenon. Figure 12a compares the deformation in two saturated samples of Darley Dale sandstone at the same effective pressure conditions but with pore pressures fixed at 10 MPa and room pressure, respectively. The two sets of data basically coincide, indicating that the effective stress principle applies and the weakening effects observed in our samples are primarily due to chemical effects and not to any complex mechanical interactions. Figure 12b also shows three tests with saturation ranging from 15% to 100%. A moderate strengthening effect was observed in the sample with only 15% saturation, which can be attributed to surface tension. The effect is somewhat smaller than that observed by *Schmitt et al.* [1994] for uniaxial compression of Fontainebleau sandstone and by *Colback and Wiid* [1965] in another quartzitic sandstone. It would be of interest to elucidate this behavior in a future study.

5. Conclusion

In this paper, we have shown that it is possible to consistently interpret the apparent differences in the weakening effect of water in the cataclastic flow and brittle faulting regimes, using micromechanical models based on the reduction of the specific surface energy in a fluid environment, as characterized by the parameter λ. On one hand, the weakening effect of water on the yield stress is proportional to $\lambda^{3/2}$ in the compactive cataclastic flow regime. On the other hand, the brittle strength in the presence of water is lowered by the ratio $\lambda^{1/2}$.

We have systematically studied the chemical influence of water on the mechanical behavior of the Berea, Boise, Darley Dale, and Gosford sandstones of different modal compositions, with porosities ranging from 11% to 35%. The water-weakening effects in the cataclastic flow regime can be explained by reductions of the specific surface energy with λ values ranging from 0.79 to 0.97. We also obtained data on water-weakening effects in the brittle faulting flow regime for the Berea and Darley Dale sandstones, which can be explained by values of λ almost identical to those inferred for the cataclastic flow behavior. Our data also indicate that the friction coefficients for sliding on preexisting crack surfaces are somewhat lower in the presence of water, and this effect contributes as well to the reduction of the brittle strength.

Acknowledgments. We are grateful to Stephen Cox and Philip Meredith, who provided the sandstone samples. We have benefited from discussion with Yves Bernabé, Joanne Fredrich, Philip Meredith, Xiang Yang Wu, and Veronika Vajdova. Constructive and insightful comments were provided by Ernie Rutter and an anonymous reviewer. This research at Stony Brook was partially supported by the Office of Basic Energy Sciences, Department of Energy under grants DE-FG-02-94ER14455 and DE-FG02-99ER14996. The research at Woods Hole was partially supported by the National Science Foundation under grant EAR-9814796.

References

Ashby, M.F., and C.G. Sammis, The damage mechanics of brittle solids in compression, *Pure Appl. Geophys.*, *133*, 489-521, 1990.

Atkinson, B.K., and P.G. Meredith, Experimental fracture mechanics data for rocks and minerals, in *Fracture Mechanics of Rock*, edited by B.K. Atkinson, pp. 477-525, Academic, San Diego, Calif., 1987.

Baud, P., and P.G. Meredith, Damage accumulation during triaxial creep of Darley Dale sandstone from pore volumometry and acoustic emission, *Int. J. Rock Mech. Min. Sci. Geomech. Abstr.*, *34*, 371, 1997.

Baud, P., and T. Reuschlé, A theoretical approach to the propagation of interacting cracks, *Geophys. J. Int.*, *130*, 460-468, 1997.

Baud, P., T. Reuschlé, and P. Charlez, An improved wing crack model for the deformation and failure of rock in compression, *Int. J. Rock Mech. Sci. Geomech. Abstr.*, *33*, 539-542,1996.

Bernabé, Y., and W.F. Brace, Deformation and fracture of Berea sandstone, in *The Brittle-Ductile Transition in Rocks*, *Geophys. Monogr. Ser.*, vol. 56, edited by A. G. Duba et al., pp. 91-101, AGU, Washington, D. C., 1990.

Boozer, G.D., K.H. Hiller, and S. Serdengecti, Effects of pore fluids on the deformation behavior of rocks subjected to triaxial compression, in *Rock Mechanics 5th Symp. Rock Mech.*, edited by C. Fairhurst, pp 579-624, Pergamon, Tarrytown, N.Y., 1963.

Brace, W.F., Volume changes during fracture and frictional sliding: A review, *Pure Appl. Geophys.*, *116*, 603-614, 1978.

Charles, R.J., Dynamic fatigue of glass, *J. Appl. Phys.*, *29*, 1657-1662, 1958.

Charles, R.J., and W.B. Hillig, Kinetics of glass failure by stress corrosion, paper presented at Symposium sur la Resistence du Verre et les moyens de l'ameliorer, Union Sci. Cont. Verre, Charleroi, France, 1962.

Chester, F.M., and J.M. Logan, Implications for mechanical properties of brittle faults from observations of the Punchbowl fault zone, California, *Pure Appl. Geophys.*, *124*, 79-126, 1986.

Colback, P.S.B., and B.L. Wiid, Influence of moisture content on the compressive strength of rocks, paper presented at Rock Mechanics Symposium, Univ. of Toronto, 1965.

Cotterell, B., and J.R. Rice, Slightly curved or kinked cracks, *Int. J. of Fract.*, *16*, 155-169, 1980.

Curran, J.H., and M.M. Carroll; Shear stress enhancement of void compaction, *J. Geophys. Res.*, *84*, 1105-1112, 1979.

Dove, P.M., Geochemical controls on the kinetics of quartz fracture at subcritical tensile stresses, *J. Geophys. Res.*, *100*, 22,349-22,359, 1995.

Edmond, J.M., and M.S. Paterson, Volume change during the deformation of rocks at high pressure, *Int. J. Rock Mech. Min. Sci.*, *9*, 161-182, 1972.

Fredrich, J.T., B. Evans, and T.-f. Wong, Effect of grain size on brittle and semi-brittle strength: Implications for micromechanical modeling of failure in compression, *J. Geophys. Res.*, *95*, 10,907-10,920, 1990.

Griffith, A.A., The phenomena of rupture and flow in solids, *Philos. Trans. R. Soc. London, 221*, 163-198, 1920.

Hadizadeh, J., and R.D. Law, Water weakening of sandstone and quartzite deformed at various stress and stress rates, *Int. J. Rock Mech. Min. Sci.*, *28*, 431-439, 1991.

Handin, J., R.V. Hager, M. Friedman, and J.N. Feather, Experimental deformation of sedimentary rock under confining pressure: Pore pressure effects, *Am. Ass. Petr. Geol. Bull.*, *47*, 717-755, 1963.

Horii, H., and S. Nemat-Nasser, Brittle failure in compression: Splitting, faulting and brittle-ductile transition. *Philos. Trans. R. Soc. London*, *319*, 337-374, 1986.

Horn, H.M., and D.U. Deere, Frictional characteristics of minerals, *Geotechnique*, *12*, 319-335, 1962.

Irwin, G.R., Fracture, in *Handbuch der Physik*, vol. VI, 551-590, edited by S. Flugge, Springer-Verlag, New York, 1958.

Israelachvili, J., *Intermolecular and Surface Forces*, Academic, San Diego, Calif., 1991.

Kemeny, J.M., and N.G.W. Cook, Micromechanics of deformation in rocks, in *Toughening Mechanisms in Quasi-Brittle Materials*, edited by S. P. Shah, pp. 155-188, Kluwer Acad., Norwell, Mass., 1991.

Lajtai, Z., H. Schmidtke, and P. Bielus, The effect of water on the

time-dependent deformation and fracture of a granite, *Int. J. Rock Mech. Min. Sci. Geomech. Abstr.*, *24* (4), 247-255, 1987.

Lawn, B.R., An atomistic model of kinetic crack growth in brittle solids, *J. Mater. Sci.*, *10*, 469-480, 1975.

Lawn, B.R., *Fracture of Brittle Solids*, 2nd ed., Cambridge Univ. Press, New York, 1993.

Lockner, D.A., J.D. Byerlee, V. Kuksenko, A. Ponomarev, and A. Sidorin, Observations of quasistatic fault growth from acoustic emissions, in *Fault Mechanics and Transport Properties of Rocks*, edited by B. Evans and T.-f. Wong, pp. 3-32, Academic, San Diego, Calif., 1992.

Menéndez, B., W. Zhu, and T.-f. Wong, Micromechanics of brittle faulting and cataclastic flow in Berea sandstone, *J. Struct. Geol.*, *18*, 1-16, 1996.

Meredith, P.G., and B.K. Atkinson, Stress corrosion and acoustic emission during tensile crack propagation in Whin Sill dolerite and other basic rocks, *Geophys. J. R. Astron. Soc.*, *75*, 1-21, 1983.

Orowan, E., The fatigue of glass under stress, *Nature*, *154*, 341-343, 1944.

Paterson, M.S., *Experimental Rock Deformation - The Brittle Field*, Springer-Verlag, New York, 1978.

Read, M.D., M.R. Ayling, P.G. Meredith, and S.A.F. Murrell, Microcracking during triaxial deformation of porous rocks monitored by changes in rock physical properties, II, Pore volumometry and acoustic emission measurements on water-saturated rocks, *Tectonophysics*, *245*, 223-235, 1995.

Rehbinder, P.A., L.A. Schreiner, and K.F. Zhigach, *Hardness Reducers in Drilling*, translated from Russian, 163 p., Counc. for Sci. and Ind. Res., Melbourne, Australia, 1948.

Rice, J.R., Thermodynamics of the quasi-static growth of Griffith cracks, *J. Mech. Phys. Solids*, *26*, 61-78, 1978.

Rutter, E.H., and D.H. Mainprice, The effect of water on stress relaxation of faulted and unfaulted sandstone, *Pure Appl. Geophys.*, *116*, 634-654, 1978.

Schmitt, L., T. Forsans, and F.J. Santarelli, Shale testing and capillary phenomena, *Int. J. Rock Mech. Min. Sci. Geomech. Abstr.*, *31*, 411-427, 1994.

Tapponier, P., and W.F. Brace, Development of stress-induced microcracks in Westerly granite, *Int. J. Rock mech. Min. Sci. Geomech. Abstr.*, *13*, 103-112, 1976.

Wiederhorn, S.M., and L.H. Bolz, Stress corrosion and static fatigue of glass, *J. Am. Ceram. Soc.*, *53*, 543-548, 1970.

Wong, T.-f., Geometric probability approach to the characterization and analysis of microcracking in rocks, *Mech. Mater.*, *4*, 261-276, 1985.

Wong, T.-f., Micromechanics of faulting in Westerly granite, *Int. J. Mech. Min. Sci. Geomech. Abstr.*, *19*, 49-64, 1982.

Wong, T.-f., C. David, and W. Zhu, The transition from brittle faulting to cataclastic flow in porous sandstones: Mechanical deformation, *J. Geophys. Res.*, *102*, 3009-3025, 1997.

Wu, X.Y., P. Baud, and T.-f. Wong, Micromechanics of compressive failure and spatial evolution of anisotropic damage in Darley Dale sandstone, *Int. J. Rock Mech. Min. Sci. Geomech. Abstr.*, in press, 2000.

Zhang, J., T.-f Wong, and M.D. Davis, High pressure embrittlement and shear-enhanced compaction in Berea sandstone: Acoustic emission measurement and microstructural observation, in Rock Mechanics Contributions and Challenges, *Proc. 31st, U.S. Symp. Rock Mech.*, 653-660, 1990a.

Zhang, J., T.-f Wong, and M.D. Davis, Micromechanics of pressure-induced grain crushing in porous rocks, *J. Geophys. Res.*, *95*, 341-352, 1990b.

Zhu W., and, T.-f. Wong, Shear-enhanced compaction in sandstone under nominally dry and water-saturated conditions, *Int. J. Rock Mech. Min. Sci.*, *34*, 372, 1997.

P. Baud and T.-f. Wong, Department of Geosciences, State University of New York at Stony Brook, Stony Brook, NY, 11794-2100. (baud@horizon.ess.sunysb.edu; tfwong@notes.cc.sunysb.edu)

W. Zhu, Department of Geology and Geophysics, WHOI, Woods Hole, MA 02543. (wzhu@whoi.edu)

(Received July 30, 1999; revised March 3, 2000;
accepted March 13, 2000.)